THE PENNSYLVANIA STATE UNIVERSITY
SCHREYER HONORS COLLEGE

DEPARTMENT OF BIOMEDICAL ENGINEERING

DETERMINING EMBOLUS TRAPPING EFFICIENCY OF AN INFERIOR VENA CAVA FILTER DURING EXERCISE

JOSHUA M. RILEY
SPRING 2018

A thesis
submitted in partial fulfillment
of the requirements
for a baccalaureate degree
in Biomedical Engineering
with honors in Biomedical Engineering

Reviewed and approved* by the following:

Keefe Manning
Professor of Biomedical Engineering
Thesis Supervisor

William Hancock
Professor of Biomedical Engineering
Honors Adviser

Peter Butler
Associate Dean for Education in the College of Engineering
Faculty Reader

* Signatures are on file in the Schreyer Honors College.

ABSTRACT

Deep vein thrombosis (DVT) and pulmonary embolism (PE) affect 1 in 1,000 people in the US annually. Inferior vena cava (IVC) filter placement is performed when patients cannot undergo anticoagulation therapies for DVT/PE. IVC filters capture thromboemboli traveling through the IVC to prevent PE. Many factors can affect the trapping efficiency of an IVC filter, including filter orientation with respect to the IVC axis, IVC orientation in relationship to gravity, and ratio of clot to fluid density. To study these factors, researchers at the U.S. Food and Drug Administration (FDA) recently designed a generic IVC filter for research purposes. The objective of this study is to characterize the embolus trapping efficiency of the FDA's generic IVC filter and to generate data to validate computational simulations of the device.

This study measured the FDA generic IVC filter's trapping efficiency using rigid beads of 3.2 mm, 4.8 mm., and 6.4 mm diameters under exercise conditions. Deformable emboli, created by the coagulation of bovine whole blood, of similar sizes and shape were also tested. A Reynolds number of 1470 was chosen for infrarenal IVC flow in coordination with pre-existing literature regarding the anatomical IVC model used in this experiment.

This study characterized the embolus trapping efficiency of the FDA generic IVC filter. The trapping efficiency depends on embolus size and the iliac vein from which the embolus originates. There is a significant difference ($p < 0.05$) in the trapping efficiency of 4.8 mm diameter deformable and rigid spheres. There is also a significant difference ($p < 0.01$) in the trapping efficiency between the left and right iliac of rigid small clots and deformable small and medium clots. These results are important for the verification of existing computational models. With verification, the accuracy of patient-specific models will better predict IVC filter success and improve patient outcomes.

TABLE OF CONTENTS

LIST OF FIGURES

LIST OF TABLES

ACKNOWLEDGEMENTS

There is no feat that I have accomplished without the aid of those that have raised and supported me. I could not have completed this thesis without my family and friends that have supported me throughout college.

I would have been lost in the Artificial Heart and Cardiovascular Fluid Dynamics Laboratory if it were not for my fellow graduate and undergraduate students. I would like to thank Dr. Bryan Good and Sailahari Ponnaluri for providing me with assistance with all of my questions in lab, and Xavier Candela, for guiding me through my first year of research and leading me into my first individual research project. I would like to thank Dr. Peter Butler and Seoyoung Son for their assistance in past research projects and their expertise in microscopy. I would like to thank Dr. William Hancock and David Arginteanu for their knowledge of protein interaction and research procedures.

I would like to thank all of my professors and mentors that have encouraged and fostered my academic and personal growth throughout my college career. The opportunities that the Pennsylvania State University and the Schreyer Honors College have granted to me have shaped my college experience. I would like to recognize the Rodney A. Erickson Discovery Grant program for funding multiple summers of my research.

Most of all, I would like to thank my thesis supervisor Dr. Keefe Manning. Throughout my college career, he has played the roles of honors adviser, research adviser, field trip chaperone, professor, and will be serving as faculty marshal at my graduation in May 2018. The advice, guidance, and mentorship you have given me has molded the man I have become throughout my undergraduate career.

Chapter 1

Introduction

1.1 Deep Vein Thrombosis and Pulmonary Embolism

Venous thromboembolism (VTE) is a disorder characterized by the formation of blood clots, or thrombi, within veins. When occurring in the deep veins, this condition is described as deep vein thrombosis (DVT). DVT occurs most commonly in the lower limbs, particularly within the veins of the thighs and calves.[1] When a part of a thrombus breaks off into the blood stream, the migrating clot becomes an embolus. DVT-induced emboli travel through the inferior vena cava (IVC), right heart, and become lodged in the pulmonary arteries. The subsequent blockage of blood flow, called pulmonary embolism (PE), causes chest pain, shortness of breath, and lung damage.[1] Behind coronary artery disease and stroke, PE is the third most common cardiovascular disease.[2] Together, DVT and PE are estimated to occur in 1.17 in 1000 people and may cause over 100,000 deaths every year in the US.[3]

The pathologic coagulation of DVT occurs after long periods of sitting or standing, when low velocity blood begins to clot. Gravity plays a large role in the blood flow of the deep veins, where upward fluid velocity through the venous valve system is driven by the contraction of calf and leg muscles. DVT infrequently originates in the deep veins of the arms. Risk factors of DVT include vein injury, slow or stagnant flow, increased estrogen, obesity, chronic heart disease, and previous/family history of DVT and PE.[1]

Four major factors of thrombosis are alterations in blood flow, endothelial injury, inflammation, and hypercoagulability. Hypercoagulability, addressed by anticoagulation therapies, garners the most focus of the current treatment and prevention methods for DVT and PE. Though effective, the reduced ability of patients' blood to clot can cause increased and prolonged bleeding in cases of vessel injury.[4] The American

Heart Association, American College of Chest Physicians, and Society of Interventional Radiology recommend patients with severe VTE and contraindications to anticoagulants to receive implanted IVC filters for DVT treatment.[4,5,6] IVC filters are designed to trap emboli as they migrate through the IVC with the purpose of preventing pulmonary embolism. IVC filters can be used either in conjunction with, or in substitution of, anticoagulation therapies.

1.2 Inferior Vena Cava Filter

The inferior vena cava filter (Fig.1) is a metallic, medical device designed to trap emboli traveling through the IVC. Use of IVC filters in DVT and PE treatments is estimated to be 13-17% in the United States.[7] Trapping efficiency, mechanical endurance, and the prevention of future thrombosis are important factors for current IVC filters. There are several permanent and removable filters currently in clinical use. Each filter is chosen for a patient based on size and permanence. The ease of filter deployment is also an important factor for interventional radiologists implanting the IVC filters in their patients.

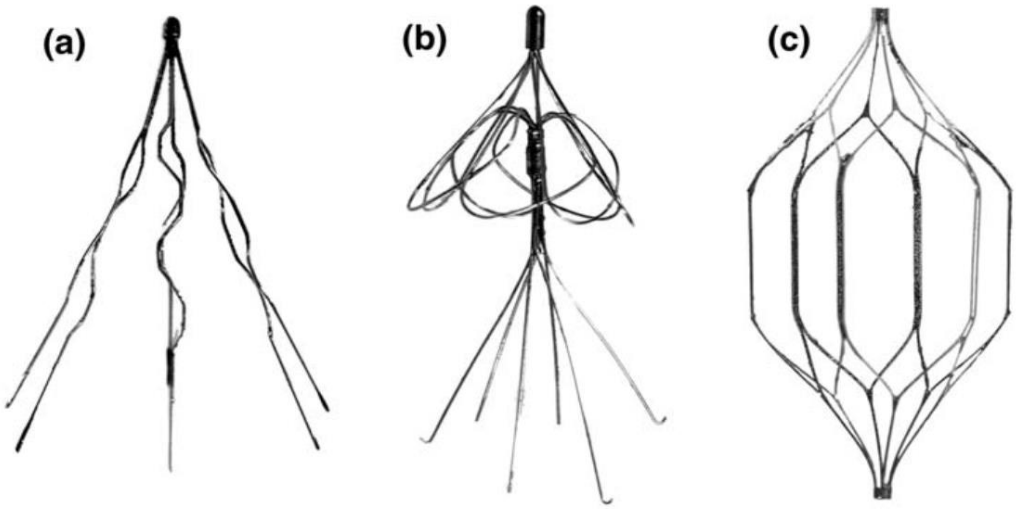

Figure 1. Three unconstrained commonly used IVC filters to demonstrate variability of design. (a) Greenfield; (b) Simon Nitinol; (c) TrapEase. (adapted from Stewart et. al.)[8]

Prior to implantation, the IVC filter is folded into a catheter. The catheter is deployed through either the internal jugular veins or femoral veins with ultrasound guidance. The catheter is moved into location

for filter deployment at the infrarenal region of the IVC. The catheter sheath is removed and the filter legs are expanded into the vena cava wall.[9] Following IVC filter implantation in the vena cava, the caval wall grows around the hooked ends of the filter struts, providing stability so the filter does not migrate or shift after implantation.

Complications occur during or after surgery in about 1-3% of IVC filter implants, including extensive clotting of the IVC, filter migration, mechanical breakage, and improper anatomic placement.[10] The complication of increased clotting within the IVC (Fig. 2) after filter implantation results in substantial morbidity. This problem occurs when an IVC filter successfully catches an embolism. However, instead of thrombus disintegration occurring, the disruption of flow patterns can cause increased thrombosis downstream of the IVC filter and on the surface of the captured clot. Methods of pharmacological and mechanical thrombolysis have been practiced to increase IVC patency with mixed success.[11,12]

Figure 2. MRI visualization of an implanted IVC filter (white arrow) in an occluded inferior vena cava. The darker grey area (black arrows) is a region of extensive thrombosis caused by the IVC filter.[13]

Another complication can occur from the mechanical injury during the IVC filter implantation. Outward radial pressure applied from the ends of the IVC struts, caused by filter deployment or physical trauma, can tear or puncture the caval wall. When a filter perforates the IVC wall, the struts can damage other internal organs, such as the duodenum, heart, and lungs.[14,15] Filter perforation through the vessel wall into the lumen of the duodenum can be seen in Figure 3. Reducing the outward force of IVC filters to reduce risk of perforation increases the chances of filter displacement and migration from high flow rates or physical trauma, potentially leading to fatal health complications.[16,17]

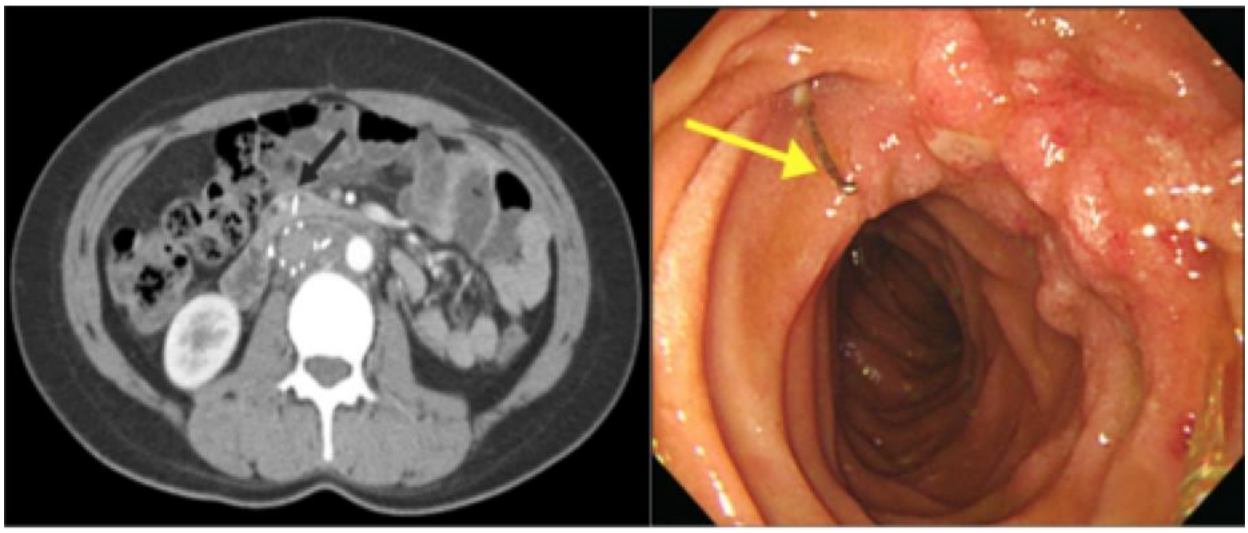

Figure 3. MRI visualization (left) of an implanted IVC filter leg (black arrow) protruding into the duodenum. Lumen endoscopy showed IVC leg (yellow arrow) protrusion and scarring on opposite side membrane (adapted from Bae *et al.*).[14]

Differences in patient anatomy during the implantation of the IVC filter can result in the placement of the IVC filter an angle with the central axis of the IVC. Angle of implantation can increase the likelihood of complication during IVC filter retrieval.[18] Large angles (>15 degrees) of tilt from the central axis of the IVC may increase the risk of emboli passing through the IVC filter, potentially causing a recurrence of PE.[19] The clot trapping efficiency, the percentage of emboli that pass through the infrarenal IVC that are captured by the filter, is an important quantification to test the efficacy of an IVC filter. This property of the IVC filter is a focus of current experimental and computational studies aimed on testing and improving IVC filter design for improved patient outcomes.

1.3 Previous IVC Filter Studies

The efficacy of IVC filters to prevent PE and caval thrombosis has been studied *in vivo, in vitro,* and *in silico*. These studies have analyzed multiple filters' effects on IVC blood flow, ability to trap emboli, and the subsequent effects on flow from the presence of a captured clot.

One of the original clinically used IVC filters, the Greenfield filter (Fig. 1a), was first tested for trapping efficiency by Thompson *et al.* (1989) in a study of seven adult sheep. Large cylindrical clots, 8 mm diameters of 10 mm and 30 mm length, were caught with one hundred percent efficiency, while smaller clots, 4 mm diameter of 10 mm and 30 mm length, were caught with 80% and 76% efficiency, respectively. As the ovine IVC diameter is similar to the human IVC, Thompson *et al.* concluded that the Greenfield filter was capable of trapping large, life threatening emboli. There was an insignificant tendency for the tilted IVC filters to trap clots less frequently than IVC filters aligned with the IVC axis.[20] This study did not account for the effect of clots already caught by the IVC filter on the outcome of subsequent thromboemboli.

A Greenfield *et al.* study (1992), coordinated by the founder of the Greenfield filter, analyzed the trapping efficiency of the IVC filter *in vitro*. Three types of Greenfield filters were implanted in dialysis tubing of three different diameters and connected to a flow loop. Four sizes of soft resin "clots" were injected into the flow loop. Multiple clots were injected in the same run, without removal of the clots already captured by the IVC filter. The overall trapping efficiency was measured at 81%, with a majority of the failures coming from smaller clots during increased flow rates to move the larger clots. This study also found that if larger emboli were released before smaller clots were injected, there was a significant increase in the likelihood the smaller clots would be caught. Though the presence of larger clots could cause an increased trapping efficiency for smaller clots, this study does not address the changes in caval flow due to

decreased patency. This study also found that there is a decrease in trapping efficiency as the vena cava increased in diameter.[21]

A study by Couch *et al*. (1997) investigated the hemodynamic effects of an occlusion within the IVC filter at a Reynolds number of 600. The study analyzed the axial velocities and shear stress distributions around an occluded and unoccluded IVC filter using a noninvasive method of flow visualization. The unoccluded filter was found to have very little effect on flow through the IVC, while occlusion creates a peripheral area of the clot with increased shear stresses. There was no turbulence or vortices observed in either filter.[22] Singer *et al*. (2009) computationally investigated the blood flow around an IVC filter. The TrapEase filter was studied under unoccluded and partially occluded conditions. These findings supported the results by Couch *et al*. (1997) that IVC filter occlusion creates areas of increased shear stresses.[23]

A numerical analysis was conducted on the Greenfield filter to study the flow dynamics and embolus trapping by Swaminathan *et al.* (2006).[24] This computational study investigated the hemodynamics of an axisymmetric, unoccluded filter at a Reynolds number of 1000. The computational model showed laminar, steady flow through the Greenfield filter and a region of stagnation downstream of the filter. This region of stagnation grew as the central hole of the IVC filter was occluded (Fig. 4). This study shows that the presence of captured clots within the IVC filter can cause disturbances in flow patterns that can increase the chance of thrombosis within the IVC and affect the future trapping efficiency of the IVC filter. This study claimed that the properties of a non-Newtonian fluid had no significant change on the flow field through and downstream of the IVC filter, though a computational study by Aycock *et al.* (2016) found that IVC simulations with Newtonian fluids over predict the Reynolds number by a factor of 2 and under-predict the wall shear stress by 28-54%, as compared to Non-Newtonian simulations.[25] As 99% of the infrarenal flow volume has shear less than 100 s^{-1}, the Aycock *et al.* (2016) study recommends simulations utilize Non-Newtonian fluids to better model hemorheological conditions within the IVC.

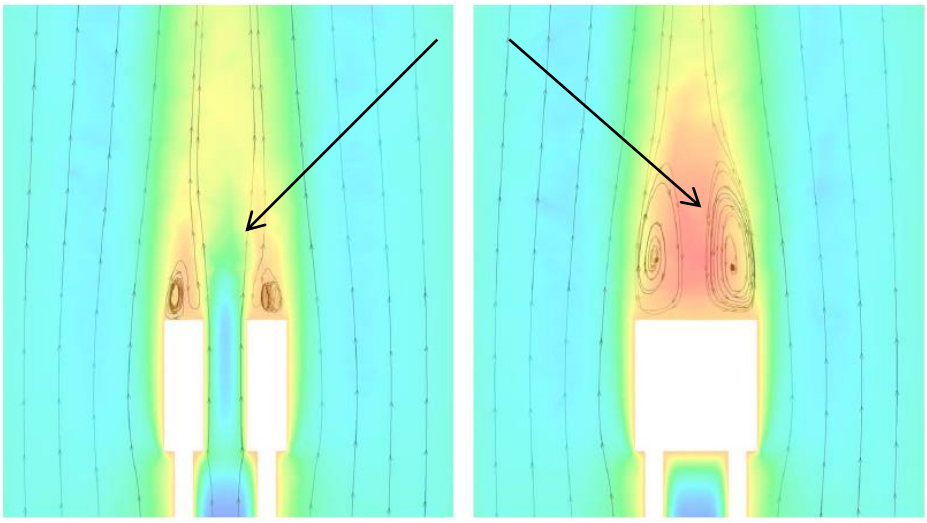

Figure 4. Flow field when the central hole of the Greenfield filter is unoccluded (left) and occluded (right).[24]

Another study, performed by Stewart *et al.* (2008), computationally and experimentally investigated the effects on flow of a thrombus present in the IVC filter at a Reynolds number of 320. The "clots" (Fig. 5) were created from polyvinyl chloride gel and tested in three different IVC filters (Fig.1). The study showed that the Greenfield filter has the least disruption in IVC flow. The study also noted that individual patient IVC characteristics are important to IVC success and should be considered when choosing the filter to be implanted. An additional finding was low wall shear stresses near the struts contact with the IVC wall. Low wall shear stresses have been previously associated with intimal hyperplasia.[8]

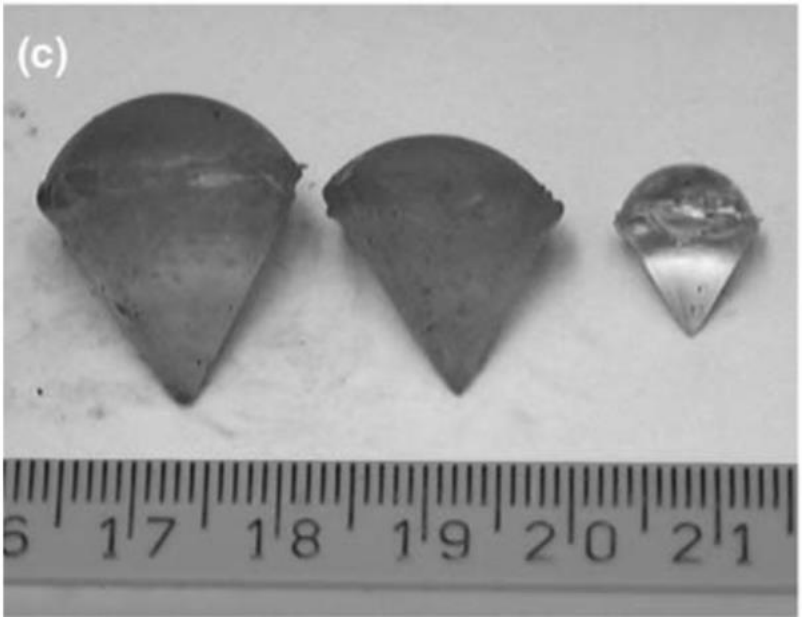

Figure 5. Conical clots used in experimental and computational study by Stewart *et al.*[8]

Another experimental flow loop study, performed by Robinson *et al.* (2013), studied the trapping efficiency of an IVC filter. The flow loop was operated at a Reynolds numbers of 340 and 490 at 37°C. The emboli injected in the flow loop were created from polyacrylamide gels (Fig. 6), ovine, and human blood. The results of this experiment yielded that stiff synthetic clots did not accurately model the trapping of emboli in an IVC filter. The comparison between the trapping efficiencies and how the clots were trapped showed that clots created from whole blood are ideal for experimental IVC filter studies.[26]

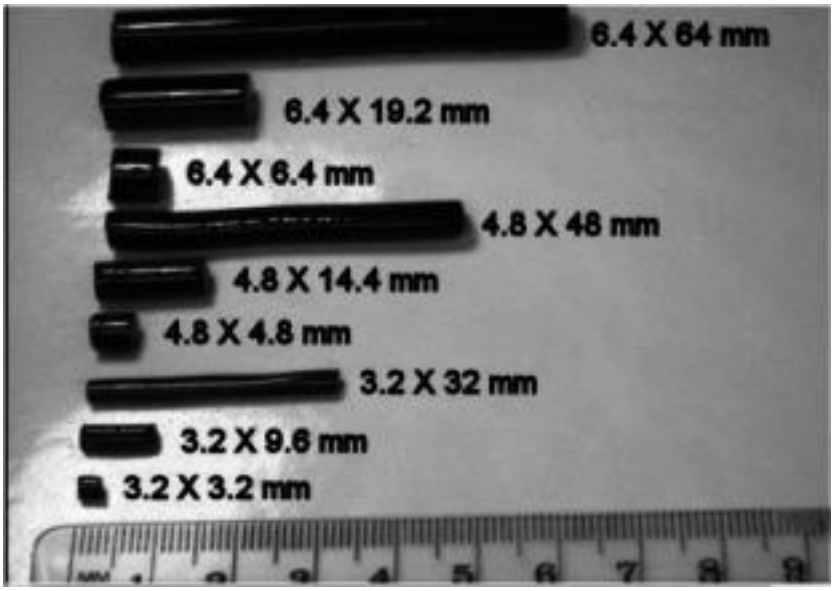

Figure 6. Polyacrylamide gel cylindrical clots used in trapping efficiency study by Robinson *et al.*[26]

To computationally model the trapping efficiency of an IVC filter, Aycock *et al.* (2017a) developed a computational fluid dynamics (CFD) model coupled with a 6-degree-of-freedom (6-DOF) simulation. This study found that 4, 5, and 6 mm diameter rigid clots with a clot-to-fluid density greater than one have nearly 100% trapping efficiency for both tilted and axial IVC filters in a vertical orientation. When the clots are made neutrally buoyant, the trapping efficiency significantly decreases.[27] Another study performed by Aycock *et al.* (2017b) analyzed IVC filters' trapping efficiency of 3 mm and 5 mm spheres in supine and vertical orientation. The study showed that filter orientation and patient IVC anatomy both had significant influence on the trapping efficiency.[28] By implanting an IVC filter in a similar experimental model of these computational studies, experimental results can help verify the results of the studies by Aycock *et al.* (2017a, 2017b).[27, 28]

1.4 Objective

The objective of this experiment is to determine the trapping efficiency of the FDA General IVC filter with non-deformable and deformable clots of multiple sizes and shapes under exercise conditions and to track the movement of clots through the IVC before and during capture by the IVC filter. A variety of clot sizes and shapes chosen from previous literature will be injected into a mock circulatory loop containing a physiological IVC model with mock iliac veins. The IVC filter trapping efficiency under high flow rates, consistent with exercising physiological values, will be tested for both iliac veins and types of emboli. These data will be used to verify the computational model put forth by Aycock *et al.* 2017a, 2017b, in conjunction with the U.S. Food and Drug Administration to guide the creation of IVC filter computational models to better predict patient outcomes.

Chapter 2

Methods

2.1: Flow Loop Design

The experimental flow loop consists of a fluid reservoir, pump, clot injection valve, and an inferior vena cava model including the left and right iliac veins. This flow loop (Fig. 7) is constructed to simulate the entrance of a clot from the iliac veins into the IVC. The IVC model was mounted vertically 1.8 meters above the ground on an optical breadboard.

Flow was driven through the loop using a variable centrifugal pump (Cole-Parmer, Vernon Hills, IL). The reservoir was connected to the pump by 0.9 m of Tygon® flexible PVC 9.5 mm diameter tubing (Saint Gobain, Courbevoie, France). Fluid from the pump traveled through 0.6 m of tubing to a Y junction, which branched identical tubing of 0.45 m length to T-junctions containing ball valves. Clots were injected into the valve systems, allowing entrance through the right or left iliac vein to be chosen for each embolus. The valve T-junctions connected to 1.1 m of Tygon® flexible PVC tubing into 1.2 m of hard, transparent PVC 24.3 mm diameter tubing (Harvel, Easton, PA) that served as an entrance length into the IVC model (Fig. 8). The total volume of the flow loop was 4 liters.

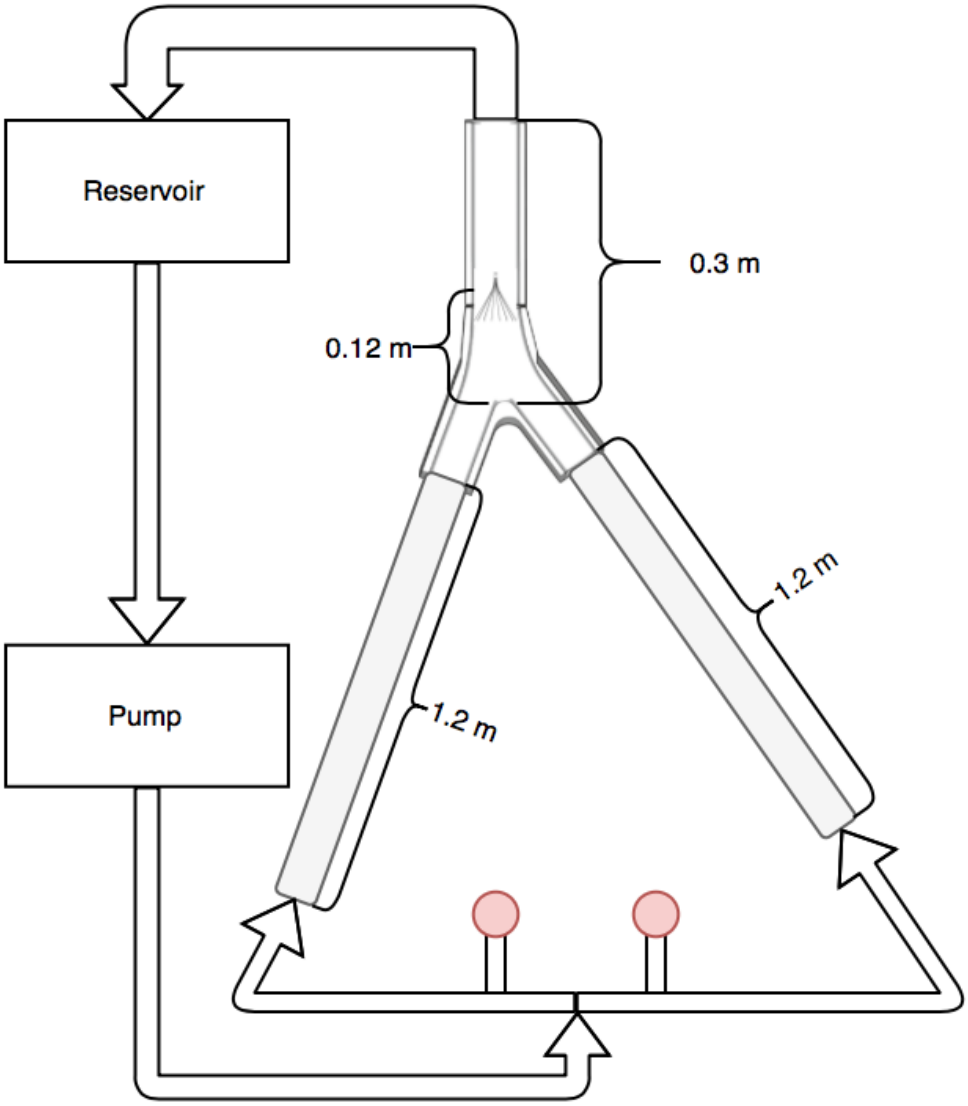

Figure 7. Flow Loop diagram – Red dots are clot injection points to choose left or right iliac vein clot entrance

The iliac veins of the IVC model begin as a circular cross section with diameter of 2.43 cm. The cross section gradually changes to elliptical as it enters the IVC portion of the model. The 30 cm length of the IVC model has a physiological elliptical cross section (Fig. 8c). The cross section of the infrarenal segment of the IVC model is 28 mm, greater than the mean physiological IVC diameter of 23 mm reported by Cheng *et al.*[29] This 21% increase in IVC diameter provides a "worst-case" scenario for clot trapping.

The antero-posterior curve of the IVC is also exhibited in this model (Fig. 8b). The IVC model was created using PolyJet 3D inkjet printing with a clear VeroClear resin sanded for smoothing and increased transparency (Fig. 8d). The index of refraction (IOR) of the model is reported at 1.5063 by Song *et al.* (2016).[30]

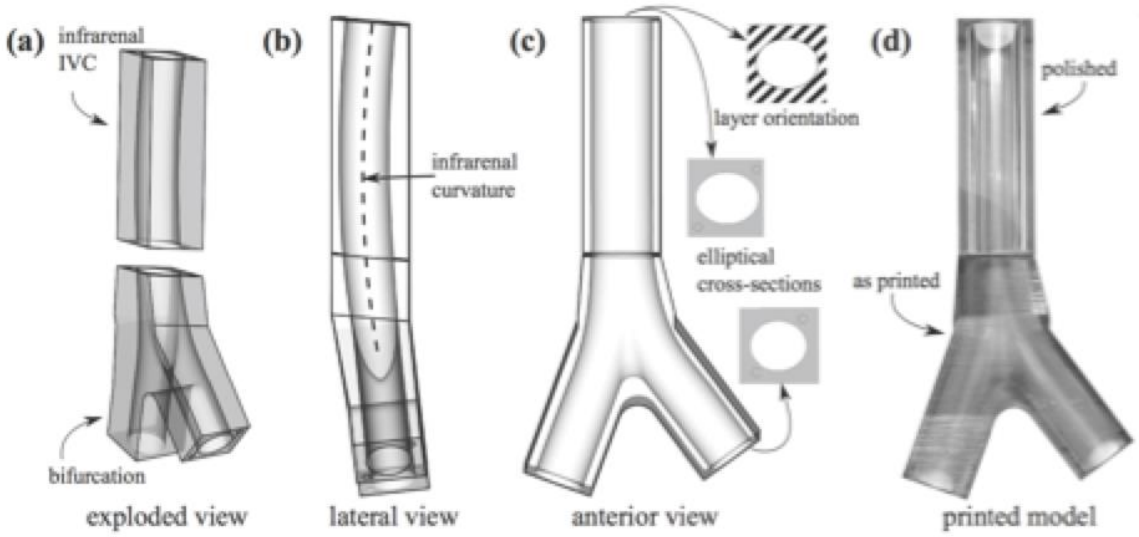

Figure 8. IVC model used in flow loop before implantation of IVC filter (adapted from Aycock et. al. (2017)).[31]

The generic FDA IVC filter (Fig. 9) is made of nitinol and consists of 16 identical struts equally spaced in a conical fashion around the hub. The hub contains a circular hole to minimize disruption of the IVC flow. The largest filter gap size for embolus escape is 5 mm, located between the ends of each strut.

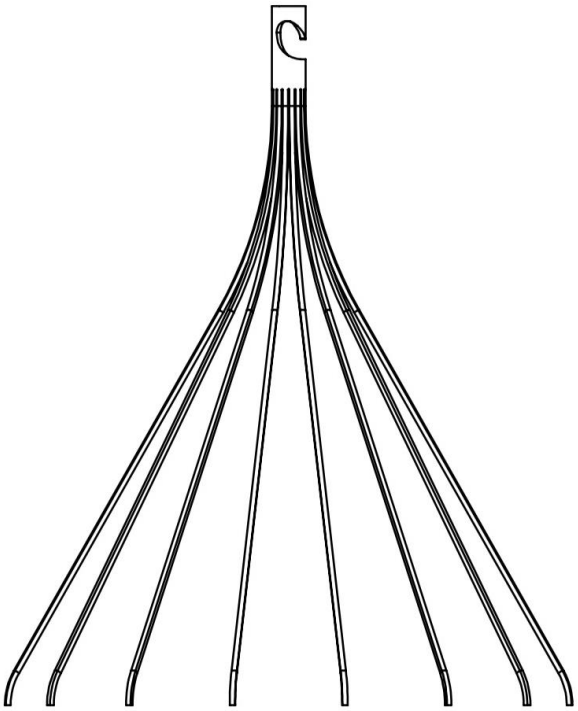

Figure 9. Generic FDA IVC Filter

The height of the implanted filter (Fig. 10) from the ends of the strut to the hub is 38 mm. The filter was implanted 120 mm above the bifurcation of the iliac veins and 70 mm above the beginning of the accessible infrarenal IVC region of the model. The hooks at the bottom of the filter were removed and cyanoacrylate was applied to the ends of the struts. After curing of the cyanoacrylate, the stability of the IVC filter was proven by subjection to flow with a Reynolds number of 3000 and the impact of a 6.4 mm diameter nylon bead.

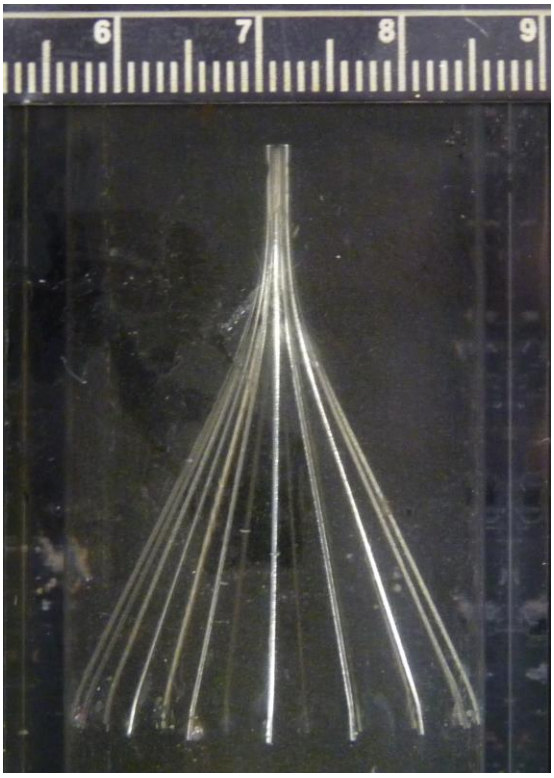

Figure 10. IVC Filter implanted in model with index of refraction matched fluid (IOR – 1.52).

2.2: Model Parameters

To accurately model and characterize embolus migration through the IVC, proper physiological conditions must be maintained within the model and flow loop. Flow conditions must be dynamically similar to a physiological IVC. The emboli injected into the model to test IVC filter trapping efficiency should have a density approximately 1-2% greater than that of the water/glycerin solution. For the rigid spheres made of nylon (density, ρ = 1.14 g/mL, modulus of compression = 2.3-2.9 GPa), a 40% glycerin/60% water by weight solution, containing 24 g/L NaCl (ρ = 1.12 g/mL, kinematic viscosity, ν = 3.24 cSt) was used to achieve this ideal clot-to-fluid density ratio.[31,32] For the deformable bovine blood clots (ρ = 1.10 g/mL, modulus of compression = 5.5 ± 2.0 kPa), a 35% glycerin/65% water by weight solution (ρ = 1.088 g/mL, kinematic viscosity, ν = 2.61 cSt) was used.

To properly visualize the migration of the embolus, the portion of the model prior to and at the IVC filter was transparent from the front and side view. The KODAK SR-Ultra Motion Corder camera (Red Lake MASD, San Diego, CA) was mounted sideways to observe the direction of flow from left to right. The camera captured the front plane of the optically accessible region of the IVC model and the side view created by a mirror at a 45° angle from the model (Fig. 11). The 125 Hz frame rate of the camera was sufficient to capture the rapid movement of the emboli as it enters the transparent portion of the IVC model. Proper lighting was necessary to avoid image glare and improve emboli contrast.

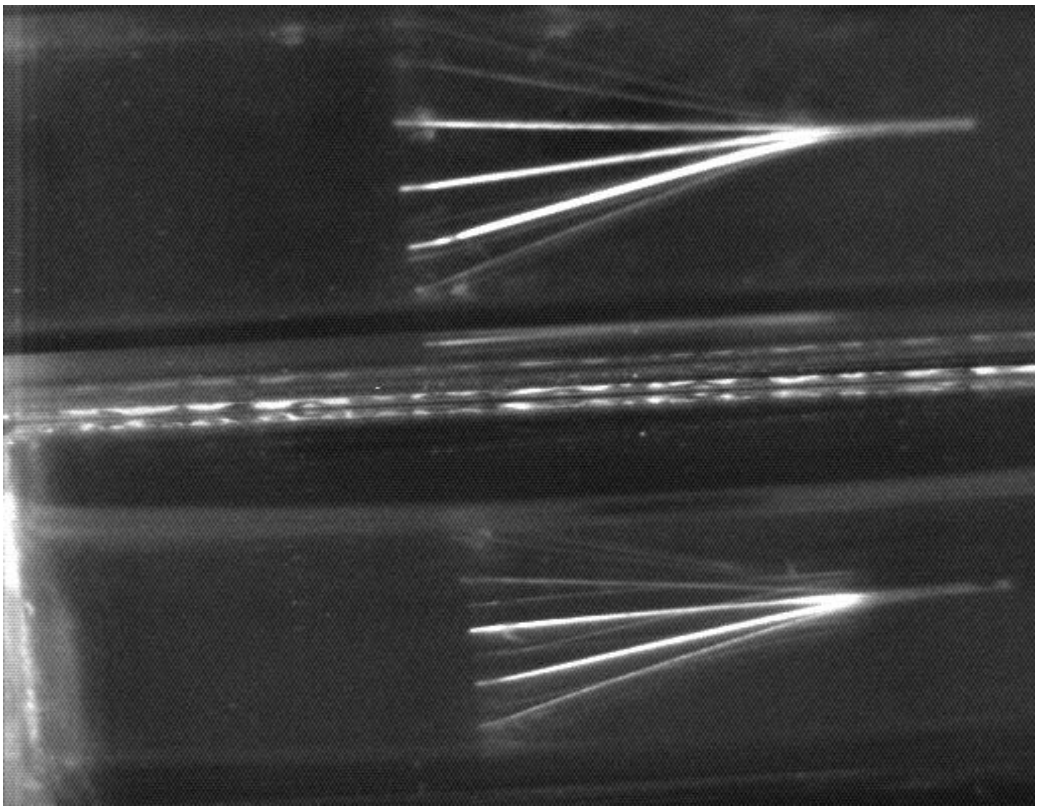

Figure 11. Front (top) and side mirror view (bottom) of the IVC filter in IVC model filled with 35% glycerin/65% water by weight solution (IOR – 1.37). Distortion of the IVC filter can be seen due to fluid/model IOR mismatch.

2.3: Physiological Considerations

Correlating the model with previous particle image velocimetry (PIV) research conditions is crucial to the applicability of this experiment. Pressure, flow rates, Reynolds number, and flow profiles all need to be considered when determining flow loop conditions.

Dynamic similarity with the PIV data from Aycock *et al*. (2017c) was achieved by matching the Reynolds number of the study's exercise flow conditions.[33] The equation for calculating Reynolds number, Re #, is:

$$Re\ \# = \frac{\rho V D}{\mu} = \frac{V * D}{\nu} \qquad \textbf{Eq. 1}$$

where ρ is fluid density, V is fluid velocity, D is the entrance diameter, μ is dynamic viscosity, and ν is kinematic viscosity. The Reynolds numbers (Table 1) were chosen to maintain dynamic similarity with PIV data for this IVC model.[33] These flow rates are higher than the physiological infrarenal IVC flow rates during exercise, reported at 5.3 ± 0.9 liters per minute (LPM), or 4.42 ± 0.75 E-5 m^3/s.[29] This supraphysiological flow rate emulates a "worst-case" scenario for IVC filter trapping efficiency.

Table 1. Flow rate calculations within the IVC model for resting and exercising conditions

	Inlet Diameter (m)	IVC Diameter (m)	Kinematic Viscosity (m^2/s)	Velocity (m/s)	IVC Flow Rate (m^3/s)	Inlet Reynolds Number	IVC Reynolds Number
Control	0.0243	0.028	3.32 E-6	0.178	1.09 E-4	848	1473
Blood Clots	0.0243	0.028	2.63 E-6	0.139	8.53 E-5	843	1463

Fully developed flow profiles were ensured by calculations of required entrance lengths. The Reynolds numbers for control and blood clots (Table 1) are both characterized as laminar flow, exhibiting Reynolds numbers less than 2300. The necessary entry length for fully developed laminar flow is determined by the diameter of the pipe and the Reynolds number of the flow, as seen in Equation 2.

$$Entrance\ Length = 0.05 * D * Re\ \# \qquad \textbf{Eq. 2}$$

The entrance lengths required for the control and blood clot exercise flow conditions are 1.03 m and 1.02 m, respectively. As the flow conditions will be simulated on the same model, the model entrance

length needs to accommodate the longest necessary entrance length. Tygon PVC hard tubing with a length of 1.2 m (4 feet) is used to create the fully developed laminar flow entering the IVC model.

2.4: Embolus Formation

Rigid nylon, spherical beads (McMaster-Carr, Elmhurst, Illinois) of sizes 3.2 mm, 4.8 mm, and 6.4 mm were selected for this study. Prior to testing, each sphere was saturated in a 40% glycerin/60% water by weight solution with 24 g/L NaCl added, and the bead's mass and diameter were measured. White beads were chosen for increased contrast in image acquisition.

The deformable emboli in this experiment were formed from reconstituted whole bovine blood obtained from the Penn State College of Agricultural Sciences through an IACUC approved procedure. The hematocrit and platelet concentrations were measured and recorded to ensure blood property consistency among samples (Table 2).

Table 2. Hematologic information of bovine samples used for blood clots

Bovine Sample	Original Hematocrit (%)	Platelet concentration (count/ mL)	Final Hematocrit (%)
1	33.3	$311 * 10^6$	50
2	29.4	$302 * 10^6$	50
3	33.3	$279 * 10^6$	50
4	30.0	$369 * 10^6$	50

Blood clot shapes and sizes were chosen to resemble nylon spheres and cylindrical polyacrylamide gels from previous literature.[26] Each bovine blood sample was used to create clots of every size and shape. Spherical molds (Fig. 12) were 3-D printed with a clear photopolymer resin using stereolithography (Formlabs, Somersville, MA). The three sizes for spherical clots were diameters of 3.2 mm, 4.8 mm, and 6.4 mm. The molds were larger than the desired diameter value, as air bubbles and coagulation led to a decrease in blood volume. The cylindrical clots were created by filling horizontal plastic tubing with bovine blood. After the blood had clotted, the tubing was cut to lengths of one (1D), three (3D), and five (5D) times

the diameter of the tubing. The density and volume of the blood clots were calculated to obtain average material values for the emboli. The blood clotting process was instigated using 10 mM calcium chloride.[34] Blood coagulated for twenty-four hours to allow for solid thrombi to form. Each clot was tested only once in this experiment.

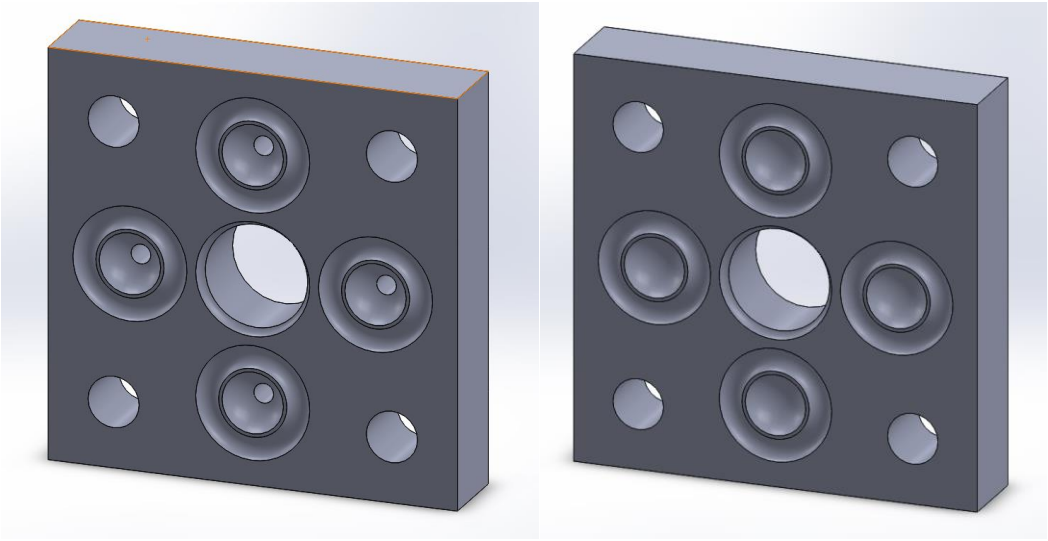

Figure 12. 3D printed resin molds for forming 3.2 mm blood clots. The top mold with port for blood injection (left) and bottom mold (right) are printed separately.

2.5: Data Collection

A Kodak SR-Ultra Motion Corder (Red Lake MASD, San Diego, CA) was used to capture the trajectories of the emboli through the IVC at a frame rate of 125 Hz. The camera was kept level with the IVC filter, focused on the front face of the IVC model. The frame encapsulated the IVC region leading into and immediately after the IVC filter. The mirror angled at 45° provides an adjacent, parallel view of this region for image acquisition (Fig. 11).

Prior to clot injection in the right or left iliac veins, the flow rates of both iliac veins were checked to ensure dynamic similarity as described in Methods 2.3: Physiological Considerations. The flow rate in each iliac vein was measured upstream of the clot injection site using a flow probe (Transonic System Inc., Ithaca, NY). Resistance clamps were used to balance flow rates between the left and right iliac veins. A pressure transducer (Argon, Athens, TX) and calibrated amplifier were used to record the pressure at the entrance of each iliac vein and 0.2 m above the IVC filter.

Emboli of each size and shape were split equally (Table 4) between injection from the right and left iliac veins for both the control and deformable blood clots within the exercise condition. The flow rate, pressure, entrance location (left or right iliac vein), and filter trapping success were recorded for each sample. Prior to injection, the mass and size of all bovine clots were measured after saturation in a 35% glycerin/65% water by weight solution. Emboli were introduced into the flow conditions through injector systems connected to the flexible PVC tubing prior to the entrance length tubes on the right and left sides. The injector system consisted of two valves connected by 25 mm of hard PVC tubing (9.5 mm diameter). The clot-to-fluid density ratio ensured the clots would sink through the tubing column filled with fluid. The clots entered into the flow field prior to the entrance length tubing. High-speed video was initiated as the embolus approached the iliac bifurcation of the IVC. Each video was limited to four seconds by the camera system. The data recorded by high-speed video software was transferred to imaging software for the analysis of video images.

Table 3. Sample size for each type of embolus tested.

	Nylon Beads			Bovine Spherical Clots			Bovine Cylindrical Clots
Iliac Vein	3.2 mm	4.8 mm	6.4 mm	3.5 mm	4.8 mm	6.0 mm	
Left	25	15	15	20	15	14	18
Right	25	15	15	20	15	14	28

The trapping efficiency of the IVC filter was converted to a percentage with a 95% exact binomial confidence interval. Differences in IVC filter trapping efficiencies based on type of clot, size, and iliac vein

were determined using a two-proportion z-test (Equation 3), where $\hat{p}_1$ and $\hat{p}_2$ are the two proportions being compared, $\hat{p}$ is the combined proportion of the two means, and n_1 and n_2 are the sample sizes of the two proportions. Significance levels of p = 0.05 and p = 0.01 were tested to determine differences in trapping efficiency percentages.

$$Z = \frac{(\hat{p}_1 - \hat{p}_2)}{\sqrt{\hat{p} * (1 - \hat{p}) * (\frac{1}{n_1} + \frac{1}{n_2})}} \qquad \textbf{Eq. 3}$$

Chapter 3

Results

3.1 Embolus Characteristics

The average density of the nylon beads was determined to be 1.14 ± 0.01 g/mL. This density corresponded to an average clot-to-fluid density ratio of 1.020. The diameters of the three bead sizes were 3.17 ± 7 E-3 mm, 4.74 ± 0.01 mm, and 6.31 ± 0.02 mm, for the 3.2 mm, 4.8 mm, and 6.4 mm beads, respectively. The molds for bovine clots yielded consistent, spherical clots (Fig. 13) of diameters similar to the nylon control beads.

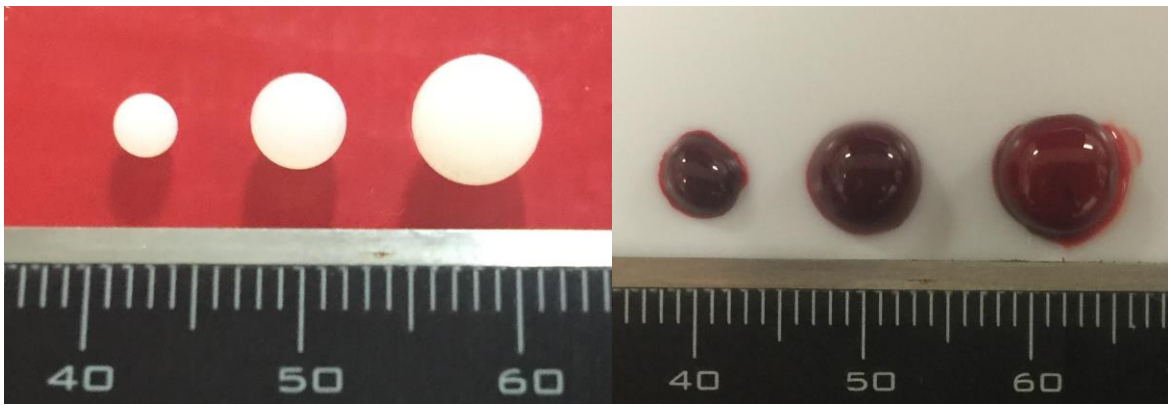

Figure 13. Examples of the small, medium, and large nylon beads (left) and bovine spherical clots (right). Bovine spherical clots appear oblong due to clot deformability. Scale bars in mm.

The densities of the small, medium, and large bovine blood clots (Table 4) provided clot-to-fluid density ratios of 1.021, 1.022, and 1.015, respectively.

Table 4. Characteristics of spherical bovine clots used for testing of the IVC filter.

	Small		Medium		Large	
	Clot Diameter (mm)	Density (g/cm^3)	Clot Diameter (mm)	Density (g/cm^3)	Clot Diameter (mm)	Density (g/cm^3)
Mean	3.548	1.111	4.898	1.112	6.071	1.104
Standard Deviation	0.201	0.011	0.231	0.012	0.309	0.010

The density of the bovine cylindrical clots (Fig. 14) could not be accurately measured due to the inconsistency of cylinder diameter throughout the clots' lengths. All cylindrical bovine clots sunk in the valve column with fluid of 1.088 g/mL density, ensuring a clot-to-fluid density greater than one.

Figure 14. Examples of the bovine whole blood cylindrical clots. Sizes are 5.3 mm 5D (top), 5.3 mm 3D (middle), and 5.3 mm 1D (bottom).

3.2 Flow Observations

The nylon beads (n=110) were tested at an average Reynolds number of 1473. The average flow rate of the left iliac, right iliac and IVC were 3.28 ± 0.05 LPM, 3.28 ± 0.05 LPM, and 6.56 ± 0.09 LPM, respectively. The average pressure at the iliac vein entrances was 50.4 ± 1.9 mmHg and 52.0 ± 2.8 mmHg for the left and right iliac veins, respectively. The pressure at the IVC filter hub was 26.2 ± 2.3 mmHg. All

beads entered the iliac veins through the center region of the circular cross section, except for the 3.2 mm diameter beads originating from the left iliac vein. A majority of the 3.2 mm nylon spheres migrated to the bottom of the flow through the entrance length tube and rolled towards the IVC bifurcation.

The spherical bovine clots (n=100) were tested at an average Reynolds number of 1460. The average flow rate of the left iliac vein, right iliac vein, and IVC were 2.56 ± 0.07 LPM, 2.56 ± 0.06 LPM, and 5.12 ± 0.13 LPM, respectively. The average pressure at the iliac vein entrances was 50.9 ± 4.37 mmHg and 55.7 ± 4.8 mmHg for the left and right iliac veins, respectively. The pressure at the IVC filter hub was 21.5 ± 4.7 mmHg. All spheres entered the iliac veins through the center region of the circular cross section, except for the smallest diameter clots in the left iliac vein. A majority of the 3.5 mm bovine blood spheres rolled up the left entrance length tubing towards the IVC bifurcation.

The cylindrical bovine clots (n=46) were tested at an average Reynolds number of 1470. The average flow rate of the left iliac vein, right iliac vein and IVC were 2.52 ± 0.02 LPM, 2.52 ± 0.05 LPM, and 5.04 ± 0.06 LPM, respectively. The average pressure at the iliac vein entrances was 51.6 ± 1.2 mmHg and 48.5 ± 1.5 mmHg for the left and right iliac veins, respectively. The pressure at the IVC filter hub was 20.6 ± 1.8 mmHg. The cylindrical clots exhibited a variety of movement habits through the entrance length tubing and iliac veins. Flow was momentarily occluded to stimulate migration for cylinders that became stuck along the entrance length tubing.

3.3 Embolus Trapping Efficiency

This study produced results of trapping efficiency of the FDA generic IVC filter based on embolus size, shape, deformability, and iliac vein of origin. The total trapping efficiency (Fig. 15) for small spherical clots, defined as emboli with diameters less than 4 mm, was 42% for rigid nylon beads (21 for 50, 95% Confidence Interval – 27.0% to 59.1%) and 42.5% for deformable blood clots (17 for 40, 95% CI – 26.5% to 66.6%). The trapping efficiency for large spherical clots, defined as emboli with diameters greater than

5.5 mm, was 100% for both rigid nylon beads (30 for 30, 95% CI – 88.4% to 100%) and deformable blood clots (28 for 28, 95% CI – 87.6% to 100%). The IVC filter trapping efficiency for medium spherical clots, with diameters between 4 mm and 5.5 mm, was 100% for rigid nylon beads (30 for 30, 95% CI – 88.4% to 100%) and 80% for deformable blood clots (24 for 30, 95% CI – 61.4% to 92.2%).

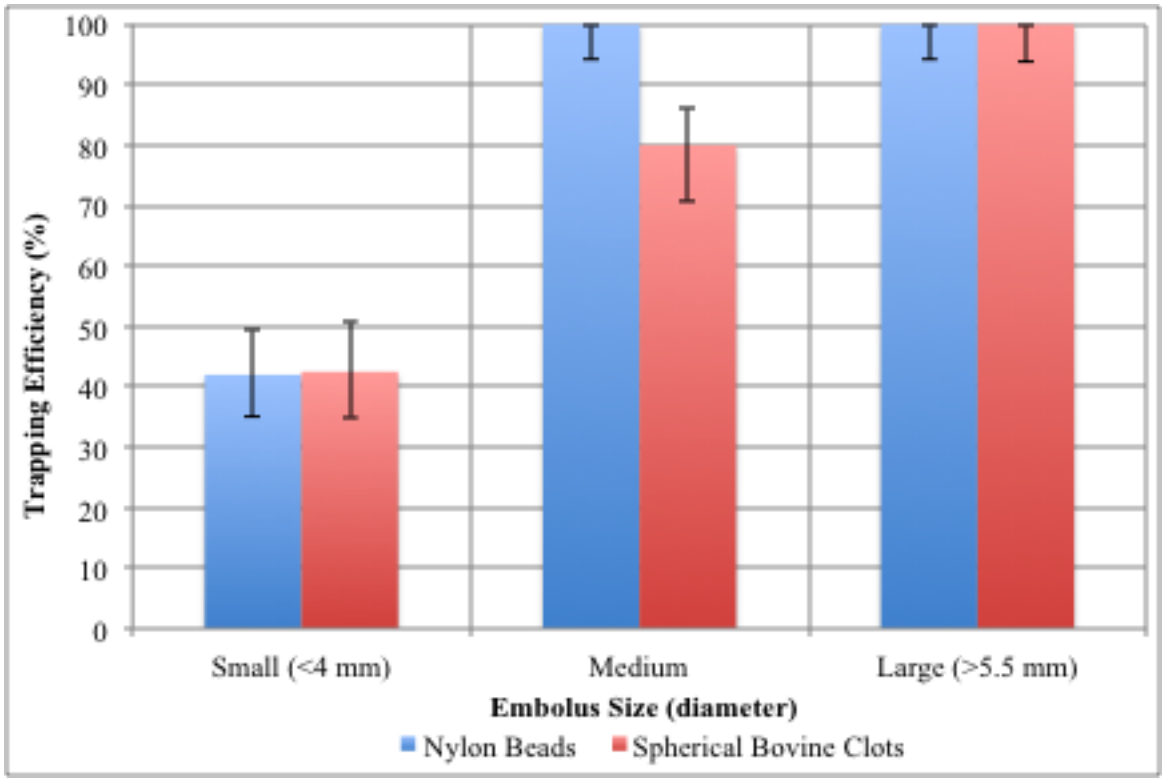

Figure 15. Embolus trapping efficiency of small, medium, and large nylon beads and bovine spherical clots, categorized by diameter. Error bars represent one standard deviation calculated from exact binomial confidence intervals.

The 3.2 mm diameter nylon beads (Fig. 16) were trapped by the IVC filter at 76% (19 for 25 caught, 95% Confidence Interval – 54.9% to 90.6%) from the left vein and 8% (2 for 25, 95% CI- 0.98% to 26.0%) from the right iliac vein. The 4.8 and 6.4 mm diameter nylon beads were caught by the IVC filter at 100% (15 for 15 each, 95% Confidence Interval - 78.2% to 100%) from the left and right iliac veins.

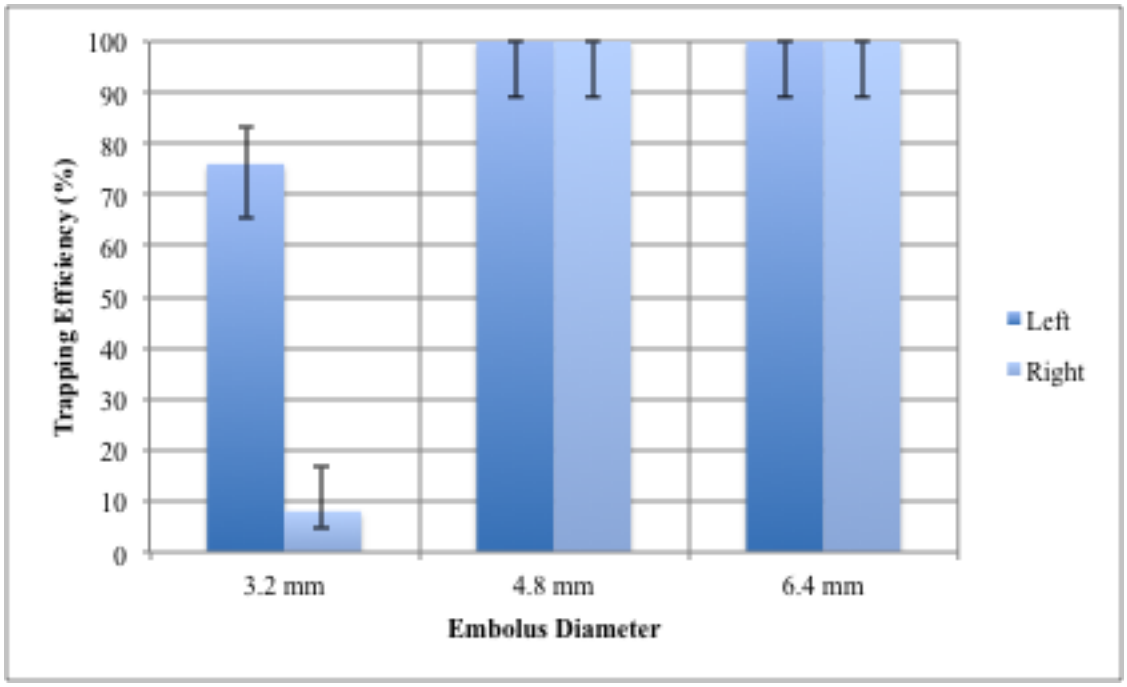

Figure 16. Embolus trapping efficiency of 3.2 mm, 4.8 mm, and 6.4 mm nylon spheres originating from the left or right iliac veins. Error bars represent one standard deviation calculated from exact binomial confidence intervals.

The 3.5 mm diameter spherical bovine clots (Fig. 17) were caught by the IVC filter at 75% (15 for 20, 95% CI – 50.9% to 91.3%) from the left iliac vein and 10% (2 for 20, 95% CI- 1.2% to 31.6%) from the right iliac vein. The 4.8 mm spherical bovine clots were caught by the IVC filter at 93.3% (14 for 15, 95% CI – 68.1% to 99.8%) from the left iliac and 66.6% (10 for 15, 95% CI, 38.4% to 88.2%) from the right iliac vein. The 6.0 mm diameter bovine clots were caught by the IVC filter at 100% (14 for 14 each, 95% CI – 76.8% to 100%) from the left and right iliac veins. The bovine clot and nylon trapping efficiencies are compared by iliac vein of origin in Figure 18.

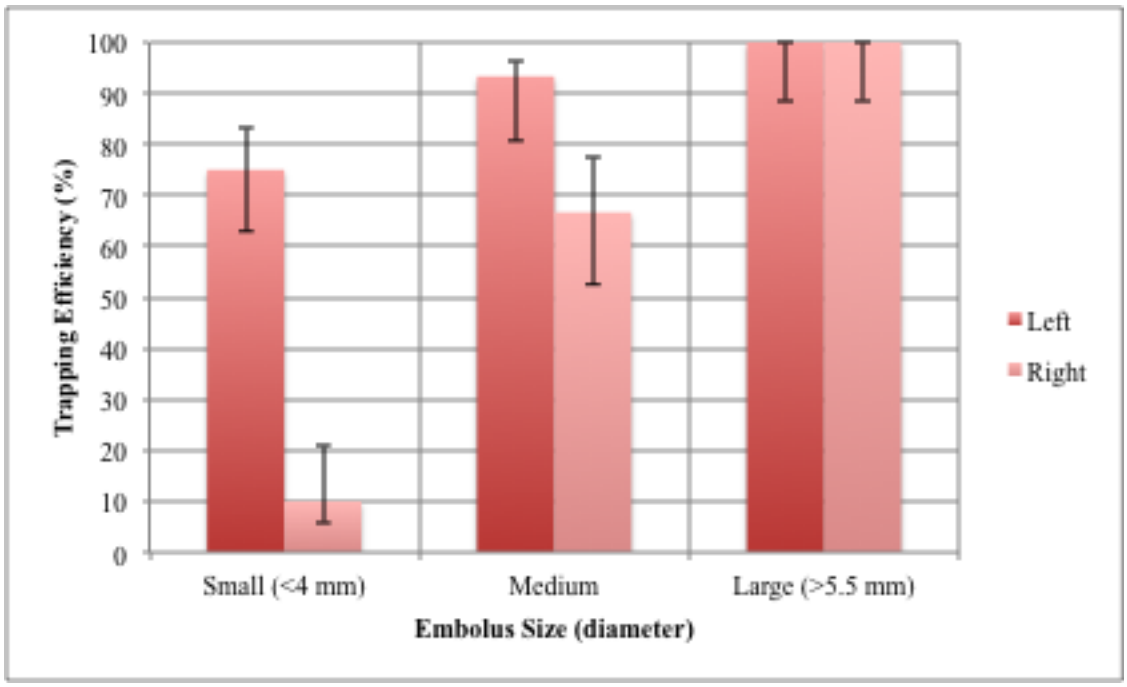

Figure 17. Embolus trapping efficiency of small, medium, and large bovine spherical clots originating from the left or right iliac veins. Error bars represent one standard deviation calculated from exact binomial confidence intervals.

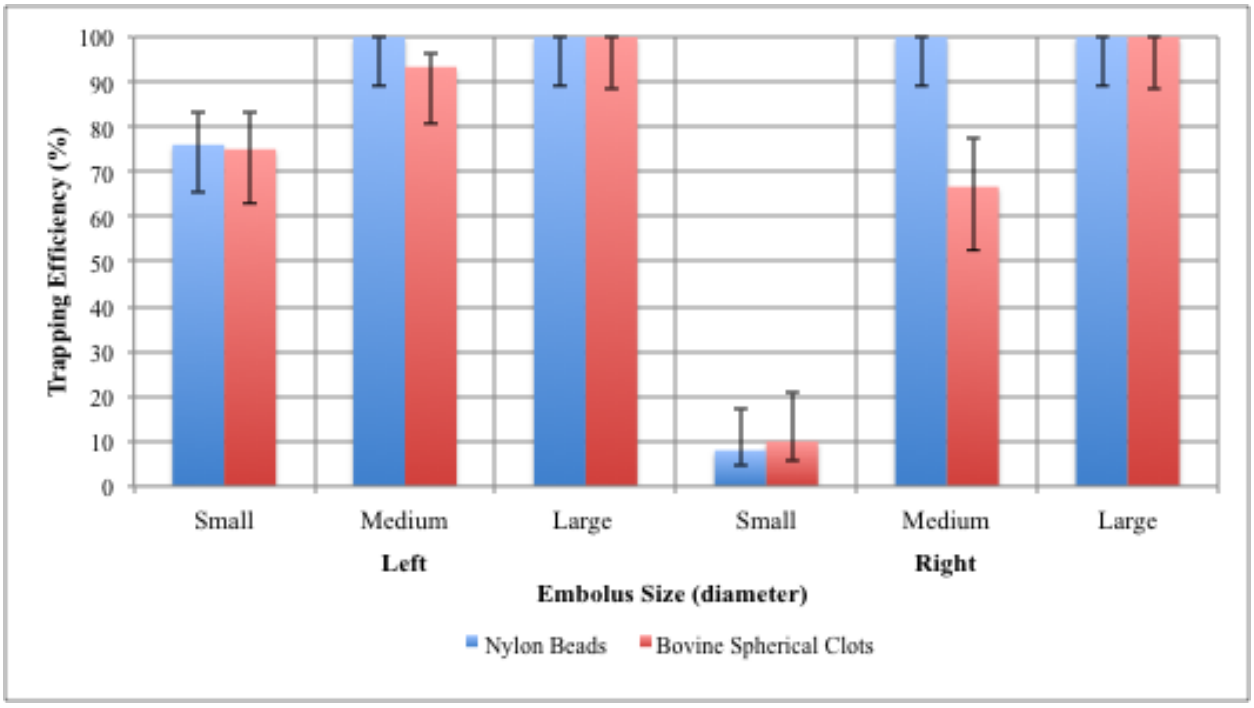

Figure 18. Embolus trapping efficiency of small, medium, and large nylon and bovine spheres, categorized by diameter and separated by the iliac vein of origin (left or right). Error bars represent one standard deviation calculated from exact binomial confidence intervals.

The cylindrical bovine clots were caught with trapping efficiencies (Table 5) varying by size and side of flow entry. All clots with a length of three and five times that of the clot diameter were caught by the filter (26 for 26). The 4.3 mm and 5.3 mm diameter clots with a length of 1x were trapped at an efficiency of 60% from the right iliac vein (6 for 10, 95% CI- 26.2% to 87.8%) and 100% from the left iliac vein (6 for 6, 95% CI- 54.1% to 100%).

Table 5. Results of IVC filter trapping with different sizes of cylindrical bovine blood clots.

	2.6 mm 3D length	2.6 mm 5D	4.3 mm 1D	4.3 mm 3D	4.3 mm 5D	5.3 mm 1D	5.3 mm 3D	5.3 mm 5D
L Trapping Success	NA	3 for 3	1 for 1	1 for 1	2 for 2	5 for 5	2 for 2	4 for 4
R Trapping Success	2 for 2	3 for 3	3 for 5	4 for 4	2 for 2	3 for 5	3 for 3	4 for 4

Note: The left trapping success is not available for 2.6 mm 3D length clots due to stalling of clots in the entrance length tubing

Chapter 4

Discussion

4.1 Discussions of Results

The results of this study showed significant differences in IVC filter trapping efficiency based on the embolus size, iliac vein of origin, and rigidity of the clot. These data match the findings of previous literature focused on the capture efficiency of IVC filters.

4.1.1 Size

There was a notable trend in increasing trapping efficiency with an increase in size. The trapping efficiency of the IVC filter of 3.2 mm nylon beads (42%) was significantly different ($p < 0.01$) than the trapping efficiency of the 4.8 mm (100%) and 6.4 mm (100%) nylon beads. There was a significant difference ($p < 0.01$) between the deformable small (42.5%), medium (80%), and large (100%) emboli. As the size of the embolus increases, the chances of filter escape decreases. The maximum filter gap size of approximately 5 mm is successful at catching spheres of similar size or larger, but less successful at catching spheres smaller than the maximum gap size. The smallest emboli were able to squeeze between the struts of the IVC filter, while the emboli with increased diameters would make contact with one or multiple struts and be forced upward into the hub of the filter. This trend in increasing capture efficiency with increasing radius is logical and well supported by previous literature.[20,28,36,37] Aycock *et al.* (2017b) demonstrated a similar trend that the trapping efficiency of 5 mm diameter rigid spheres was greater than the trapping efficiency of 3 mm spheres while the IVC is in an upright position.[28] This information could guide the

design of future IVC filters to minimize gap size between filter struts to increase the IVC filter trapping efficiency of smaller diameter emboli.

4.1.2 Iliac Vein of Clot Origin

The distinct angles of the left and right iliac vein with the IVC created a difference in IVC filter trapping efficiency based on the iliac vein through which the clot entered the IVC. The IVC filter trapping efficiency was significantly different ($p < 0.01$) for rigid 3.2 mm beads originating from the left (85%) and right (19%) iliac vein. The difference in trapping efficiency for deformable small spheres from the left (75%) and right (10%) iliac veins was significant at $p < 0.01$. The lesser angle of the right iliac vein created increased upwards velocity for emboli entering the IVC. This increased the likelihood of nylon and spherical blood clots escaping the IVC filter. Furthermore, the greater angle of the left iliac vein produced flow more perpendicular to that of the IVC. Small nylon beads and blood clots would roll along the bottom of the entrance length tube. The friction induced along the bottom of the tube further diminishes the upward velocity of the embolus as it enters the IVC. A minority of the emboli migrated through the center of the flow through the left entrance length tube. These clots presented a higher likelihood of escaping the IVC filter due to their increased upward velocity. Trial observations showed trends in the embolus migration for captured and escaped small nylon and blood clots (Fig. 19).

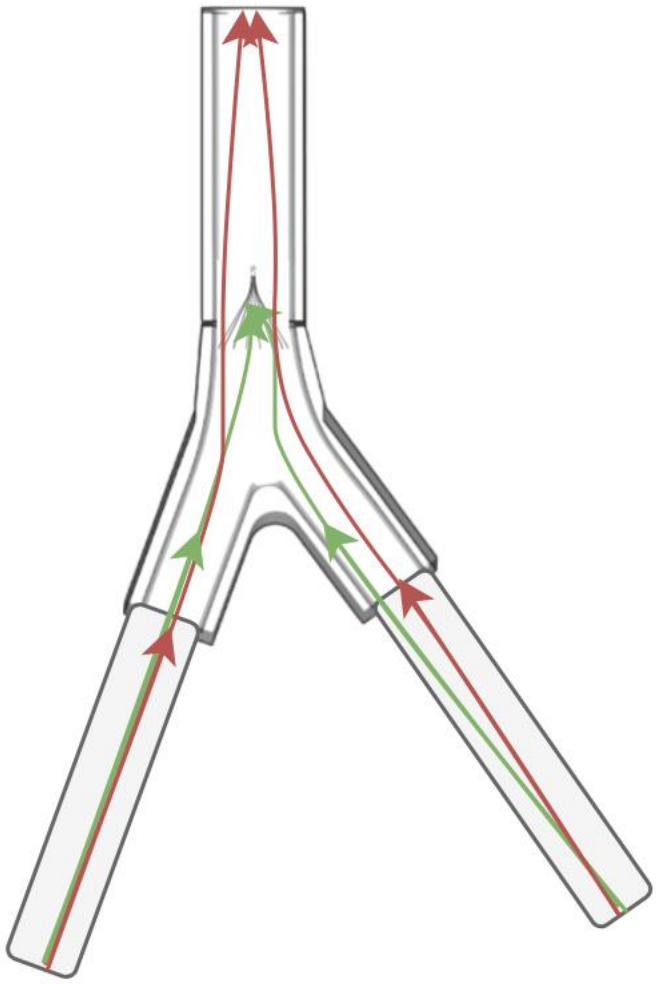

Figure 19. Tendencies in embolus migration for small clots that escaped (red arrows) and were captured (green arrows) by the IVC filter.

Aycock *et al.* (2017b) suggests that trapping efficiency is dependent on the side of clot origin, however, this study showed a trend in increased left iliac vein tapping efficiency as compared to the right side.[28] The Aycock *et al.* (2017b) study focused on an individual patient-specific anatomy, introducing flow patterns and vortices not observed in the IVC model used in this experiment. The patient-specific anatomy (Fig. 20) of the IVC in this study contained curves and grooves in the caval and iliac vein walls that induced

minor flow patterns that affected the flow field and the migration of the emboli. The distance of the IVC filter hub from the iliac vein bifurcation, 57 mm, is half that of this experiment's distance, 120 mm. The reduced distance of embolus travel through the IVC until encountering the IVC filter could cause emboli to remain in the further radial regions of the flow field. This could allow the emboli to escape between the IVC filter struts at a greater rate.

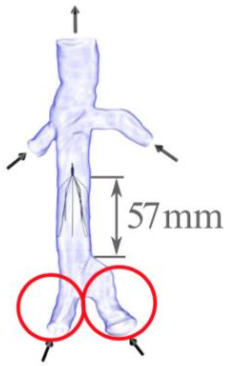

Figure 20. Patient-specific IVC anatomy studied by Aycock *et al.* (2017b). Red circles depict areas of clot injection.

4.1.3 Rigid vs. Deformable

The emboli's mechanical properties were shown to have effects on the trapping efficiency of the IVC filter. The moduli of compression for the blood clots (5.5 kPa) and nylon spheres (2.3-2.9 GPa) differed by a factor of 10^6. There was a significant difference ($p < 0.05$) in the IVC trapping efficiency of the medium sized rigid (100%) and deformable (80%) spheres originating from the right iliac (100% - rigid, 66.7% - deformable). The deformability of the spherical blood clots allowed for the clots to slide past the IVC filter struts more frequently than the nylon beads. The medium-sized rigid and deformable clots were both 4.8

mm diameter, suggesting that the difference in trapping efficiency from the right iliac was solely due to the difference in the rigidity of the clots. Small blood clots closer to the size of the 3.2 mm nylon spheres and a large sample size could lead to a similar reduced trapping efficiency of deformable clots as seen in the 4.8 mm trials.

4.2 Future Works

While this study shows significant differences in the trapping efficiency between emboli originating from the left or right iliac veins and the capture rate of medium-sized rigid and deformable clots, increasing sample size could help ensure the lack of difference in the trapping efficiencies of the small rigid and deformable clots. A lower Reynolds number flow, simulating resting conditions, should be tested to further validate computational IVC filter models. This lower flow rate should exhibit higher embolus trapping efficiencies as demonstrated by Aycock *et al.* (2017b). This IVC model could also be mounted horizontally rather than vertically, mimicking a supine orientation. This study could validate the results of Aycock *et al.* (2017b) that a horizontal IVC orientation decreases trapping efficiencies, caused by the sinking of the emboli to the outer radial area of the IVC where the gaps between struts of the filter are greater.

Procedural adjustments could be made to increase the consistency of blood clot size and density. The plasma/red blood cell separation that occurs in stagnant blood could be prevented by rotating the tubing for cylindrical clots during coagulation. Improvements in the measurements of blood cylinder density could yield the true densities of these clots. Soft polyacrylamide gels, as used in Robinson *et al.* (2013), could be added in future experiments as a comparison to the cylindrical bovine blood clots.

There are a myriad of possible projects for the flow loop created in this study. The generic FDA IVC filter could be removed from the model and replaced with other IVC filter to compare trapping efficiencies. Future studies could also utilize a fluid matching the index of refraction of the IVC model to

enable embolus tracking through the IVC. The knowledge of the migration of emboli through the IVC could provide insight into the tendencies of emboli that escape IVC filter capture.

BIBLIOGRAPHY

1. *Venous Thromboembolism*. Centers for Disease Control and Prevention, 22 June 2015, www.cdc.gov/ncbddd/dvt/data.html.
2. Belohlavek J, Dytrych V, Linhart A. Pulmonary embolism, part I: Epidemiology, risk factors and risk stratification, pathophysiology, clinical presentation, diagnosis and nonthrombotic pulmonary embolism. *Exp Clin Cardiol,* 18(2):129-38, 2013.
3. Office of the Surgeon General (US); National Heart, Lung, and Blood Institute (US). The Surgeon General's Call to Action to Prevent Deep Vein Thrombosis and Pulmonary Embolism. Rockville (MD): Office of the Surgeon General (US); 2008.
4. Kearon C, Akl EA, Ornelas, et al. Antithrombotic therapy for VTE disease. *Chest,* 149(2):315-352, 2016.
5. Jaff MR, McMurtry MS, Archer SL, et al. Management of massive and submassive pulmonary embolism, iliofemoral deep vein thrombosis, and chronic thromboembolic pulmonary hypertension: a scientific statement from the American Heart Association. *Circulation,* 123:1788-1830, 2011.
6. Caplin DM, Nikolic B, Kalva SP, et al. Quality improvement guidelines for the performance of inferior vena cava filter placement for the prevention of pulmonary embolism. *J Vasc Interv Radiol,* 22:1499-1506, 2011.
7. Alkhouli M, Bashir R Inferior vena cava filters in the United States: less is more. *Int J Cardiol,* 177(3):742-3, 2014.
8. Stewart SFC, Robinson AR, Nelson RA, et. al. Effects of Thrombosed Vena Cava Filters on Blood Flow: Flow Visualization and Numerical Modeling. *Annals of Biomed Eng,* 36 (11): 1764–81, 2008.

9. Funaki B. Inferior Vena Cava Filter Insertion. *Semin Intervent Radiol,* 23(4): 357–60, 2006.
10. Giannoudis PV, Ippokratis P, Pape HC, Patel JV. Safety and efficacy of vena cava filters in trauma patients. *Injury,* 38:7–18, 2007.
11. Kohi MP, Kohlbrenner R, Kolli KP, Lehrman E, Taylor AG, Fidelman N. Catheter directed interventions for acute deep vein thrombosis. *Cardiovascular Diagnosis and Therapy*. 6(6):599-611, 2016.
12. Protack CD, Bakken R, Patel N, Saad WE, *et al.* Long-term outcomes of catheter directed thrombolysis for lower extremity deep venous thrombosis without prophylactic inferior vena cava filter placement. *J Vasc Surg.* 45(5) 992-7. 2007
13. Evans NS, Ratchford EV. Inferior Vena Cava (IVC) Filters. *Vasc Med,* 20 (4): 382–83. 2015.
14. Bae MJ, Chung SW, Lee CW, Kim S, Song S. Duodenal perforation caused by an inferior vena cava filter. *Korean J Thorac Cardiovasc Surg,* 45(1): 69–71, 2012.
15. Nicholson W, Nicholson WJ, Tolerico P, *et al*. Prevalence of fracture and fragment embolization of bard retrievable vena cava filters and clinical implications including cardiac perforation and tamponade. *Arch. Intern Med,* 170:1827–31, 2010.
16. Peters MN, Khazi Syed RH, Katz MJ, Moscona JC, Nijjar VS, Bisharat MB. Inferior Vena Cava Filter Migration to the Right Ventricle Causing Nonsustained Ventricular Tachycardia. *Texas Heart Institute Journal*. 40(3):316-9, 2013.
17. Haddadian B, Shaikh F, Djelmami-Hani M, Shalev Y. Sudden Cardiac Death Caused by Migration of a TrapEase Inferior Vena Cava Filter: Case Report and Review of the Literature. *Clin. Cardiol.* 31: 84–87, 2008.
18. Grewal S, Chamarthy MR, Kalva SP. Complications of inferior vena cava filters. *Cardiovascular Diagnosis and Therapy*. 6(6):632-41, 2016.
19. Rogers FB, Strindberg G, Shackford SR, Osler TM, *et al*. Five-year follow-up of prophylactic vena cava filters in high-risk trauma patients. 133(4):406-11; 1998.

20. Thompson BH, Cragg AH, Smith TP, et al. Thrombus-trapping efficiency of the Greenfield filter in vivo. *Radiology,* 172(3 pt 2): 979-81, 1989.
21. Greenfield LJ, Proctor MC. Experimental embolic capture by asymmetric Greenfield filters. *J Vasc Surg,* 16(3): 436-44, 1992.
22. Couch GG, Kim H, Ojha M. In Vitro Assessment of the Hemodynamic Effects of a Partial Occlusion in a Vena Cava Filter. *Journal of Vascular Surgery,* 25 (4): 663–72, 1997.
23. Singer MA, Henshaw WD, Wang SL. Computational Modeling of Blood Flow in the TrapEase Inferior Vena Cava Filter.*Journal of Vascular and Interventional Radiology,* 20(6): 799–805, 2009.
24. Swaminathan TN, Howard HH, Patel AA. Numerical Analysis of the Hemodynamics and Embolus Capture of a Greenfield Vena Cava Filter. *Journal of Biomechanical Engineering*, 128:360–70, 2006.
25. Aycock KI, Campbell RL, Lynch FC, Manning KB. The Importance of Hemorheology and Patient Anatomy on the Hemodynamics in the Inferior Vena Cava. *Annals of Biomedical Engineering,* 44:3568–3582, 2016.
26. Robinson RA, Herbertson LH, Grossman LW, *et al.* Limitations of Using Synthetic Blood Clots for Measuring in Vitro Clot Capture Efficiency of Inferior Vena Cava Filters. *Medical Devices: Evidence and Research,* 6(1): 49–57, 2013.
27. Aycock KI, Campbell RL, Manning KB, Craven BA. A resolved two-way coupled CFD/6-DOF approach for predicting embolus transport and the embolus-trapping efficiency of IVC filters. *Biomech Model Mechanobiol,* 16(3):851–869, 2017a.
28. Aycock KI, Campbell RL, Lynch FC, Manning KB, Craven BA. Computational predictions of the embolus-trapping performance of an IVC filter in patient specific. *Biomech Model Mechanobiol,* 16(6):1957–1969, 2017b.
29. Cheng CP, Herfkens RJ, Taylor CA. Inferior vena caval hemodynamics quantified in vivo at rest and during cycling exercise using magnetic resonance imaging. *Am J Physiol Heart Circ Physiol,*

284: H1161-7, 2003.

30. Song MS, Park SH, Kim ES. Particle image velocimetry measurements of 2-dimensional velocity field around twisted tape. *Fusion Eng Des.* 109–111: 596–601, 2016.
31. "Compressive Strength Testing of Plastics." *MatWeb.com* http://www.matweb.com/reference/compressivestrength.aspx.
32. "Extruded Nylon 66." *Gemini Plastics, Inc.* http://www.gplastics.com/pdf/extruded-nylon-66.pdf.
33. Aycock KI, Hariharan P, Craven BA. Particle image velocimetry measurements in an anatomical vascular model fabricated using inkjet 3D printing. *Exp Fluids*. 58:154, 2017c.
34. Wufsus AR, Macera NE, Neeves KB. The Hydraulic Permeability of Blood Clots as a Function of Fibrin and Platelet Density. *Biophysical Journal Volume*, 104:1812–1823, 2013.
35. Pulenthiran, A. Embolus Migration and Capture from Different Cross-Sectional Release Positions. Honors BS Thesis. The Pennsylvania State University. Spring 2016.
36. Millward SB, Marsh IJ, Pon C, Moher D. Thrombus-trapping Efficiency of the LGM (Vena Tech) and Titanium Greenfield Filters in Vivo. *Journal of Vascular and Interventional Radiology.* 3(1): 103-6. 1992.
37. Jaeger HJ, Glasg SK, *et al.* In Vitro Model for the Evaluation of Inferior Vena Cava Filters: Effect of Experimental Parameters on Thrombus-Capturing Efficacy of the Vena Tech-LGM Filter. *Journal of Vascular and Interventional Radiology.* 9(3): 295-304. 1998.

Academic Vita of Joshua M. Riley
jmr6277@psu.edu

EDUCATION

exp. 05/2018 B.S. in Biomedical Engineering (Biochemical Option), Honors in Biomedical Engineering, Schreyer Honors College, The Pennsylvania State University

THESIS

04/2018 Determining Embolus Trapping Efficiency of an IVC Filter During Exercise
Thesis Supervisor: Keefe B. Manning, Ph.D.

ACADEMIC RELATED EXPERIENCES

2017-2018 Grader, BME 313 Thermodynamics for Biomedical Engineering
The Pennsylvania State University

2018-Present Grader, BME 409 Biofluid Mechanics
The Pennsylvania State University

GRANTS

Current:

Penn State Erickson Discovery Grant (PI) 5/17-8/17
Impact of Shear Rate on Von Willebrand Factor Unfolding

Completed:

Penn State Erickson Discovery Grant (PI) 5/16-8/16
Understanding Proteolysis of Von Willebrand Factor Due to Shear Rate and Presence of ADAMTS13

HONORS AND AWARDS

2017 Evan Pugh Scholar Award (Penn State)

2017 Penn State Undergraduate Exhibition Information Literacy Award – Honorable Mention

2014-2017 Gerald L. Bayles Memorial Scholarship (Penn State)

2014-2017 Academic Excellence Scholarship (Penn State)

2016 The President Sparks Award (Penn State)

2015 The President's Freshman Award (Penn State)

2014 National Merit Finalist Award

PRESENTATIONS

Riley, J.M., Candela, X.J., Hancock, W.O., Butler, P.J., Manning, K.B. Impact of Shear Rate on Von Willebrand Factor Unfolding. *2017 Summer Biomechanics, Bioengineering and Biotransport Conference*, Tucson, AZ, June 22, 2017.

Understanding Proteolysis of Von Willebrand Factor Due to Shear Rate and Presence of ADAMTS13. *2017 Undergraduate Research Exhibition*, University Park, PA, April 5, 2017.

CONFERENCE ABSTRACTS

Riley, J.M., Price, N.S., Craven, B.A., Aycock, K.I., Manning, K.B. 2018. Preliminary Study of the Embolus Trapping Efficiency of the FDA Generic IVC Filter**.** *8th World Congress of Biomechanics*, Dublin, Ireland, July 8-12, 2018.

Riley, J.M., Price, N.S., Craven, B.A., Aycock, K.I., Manning, K.B. 2018. Experimental Characterization of the Embolus Trapping Efficiency of the U.S. FDA Generic Inferior Vena Cava Filter. *Joint Meeting of The European Society for Clinical Hemorheology and Microcirculation, The International Society of Clinical Hemorheology, and The International Society of Biorheology*. Krakow, Poland, July 2-6, 2018.

Riley, J.M., Price, N.S., Craven, B.A., Aycock, K.I., Manning, K.B. 2018. An Experimental Study of the Embolus Trapping Efficiency of the FDA Generic Inferior Vena Cava Filter. *American Society for Artificial Internal Organs 64th Annual Conference.* Washington, D.C., June 13-16, 2018.

Riley, J.M., Candela, X.J., Hancock, W.O., Butler, P.J., Manning, K.B. 2017. Impact of Shear Rate on Von Willebrand Factor Unfolding. *2017 Summer Biomechanics, Bioengineering and Biotransport Conference*, Tucson, AZ, June 22, 2017.

UNIVERSITY SERVICE

The Pennsylvania State University:

Interview Committee for Dean of Schreyer Honors College, Student Leader - 2017
Interview Committee for Assistant Vice President and Assistant Dean for Undergraduate Education, Student Representative - 2016